SAND2021-15209C

Shock Tube Index of Refraction Measurements Using a Quadrature Fringe Imaging Interferometer

Gwendolyn T. Wang*, Yuzhe Peng†, Wenting Sun‡, and Yi Chen Mazumdar§
Georgia Institute of Technology, Atlanta, GA, 30332, USA

Understanding the aero-optical properties of gases is important for the study of hypersonic flows, plasmas, and other complex compressible gas phenomena. At high temperatures, the index of refraction is expected to deviate significantly from linear Gladstone-Dale constant predictions. Due to challenges associated with achieving high temperature conditions at moderate pressures and a lack of optical techniques capable of capturing changes across a discrete shock, current Gladstone-Dale estimates above 6000 K are either from theory or extrapolated from less extreme conditions. In previous work, we developed a novel quadrature fringe imaging interferometer that utilizes a narrowband and broadband source to capture large fringe changes across a discrete boundary. In this paper, we discuss improvements made to adapt and calibrate the diagnostic in shock tube environments. Then, the system is demonstrated in a diaphragm shock tube at a Mach number of 2.92. The index of refraction measured using the quadrature fringe imaging interferometer is then compared to theoretical calculations.

I. Introduction

Understanding complex non-equilibrium flow fields requires the characterization of high-temperature aero-optical properties in gases. The index of refraction properties are particularly important for estimating, validating, and correcting measurements made through hypersonic boundary layers or plasmas [1]. At low temperatures, the wavelength-dependent relationship between the index of refraction and density is captured using the Gladstone-Dale constant, also referred to as the specific refractivity [2–4]. At temperatures above 6000 K, however, theoretical calculations predict strong dependencies on pressure, temperature, and molecular polarizability due to dissociation and ionization [5]. Since these conditions are difficult to replicate and can only be achieved uniformly in high-enthalpy facilities like shock tubes, very few experiments have been attempted and no accurate validation data currently exist.

In addition, optical techniques capable of tracking large index of refraction changes across a discrete shock front at moderate to high pressures are rare. Existing experiments for making these measurements in shock tubes include 2D fringe counting [6–11], point diffraction interferometry (PDI) [12], common path interferometry [13], and angled beam refraction [14]. The sudden shift in index of refraction across a shock front can correspond to the motion of hundreds of fringes on an optical interferometer, making fringe counting challenging. Fringe counting and PDI are also limited in range, since no directional information is present for sudden discrete jumps. Common path interferometry requires an in-frame reference and cannot be used if the shock-wave is not in the field-of-view. Finally, angled beam refraction methods often require custom angled window ports as well as long beam paths.

In order to overcome the limitations of existing diagnostic methods, we developed a novel quadrature fringe imaging interferometer (QFII) [15] method to accurately identify large changes in index of refraction across a discrete shock front. Some related phase quadrature interferometer techniques exist [16–18] for making measurements of index-of-refraction changes around models in shock tubes, but have not been implemented to study dynamic shock conditions for high enthalpy flows. The QFII method combines a narrowband quadrature and finite broadband fringes to automatically track fine fringe movements, fringe movement direction, and large fringe shifts across a discrete jump. The resolution and feasibility of this technique was explored [15, 19], but experimental shock tube measurements have not been previously reported. In this paper, we first describe the diagnostic method for utilizing quadrature and finite broadband fringes for index of refraction measurements. Then we describe the two-camera calibration technique and the inversion method for calculating index of refraction from discrete images. Finally, this method is demonstrated in a single diaphragm shock tube and the experimental index of refraction is compared to theoretical calculations.

*Ph.D. Student, Woodruff School of Mechanical Engineering, gtwang@gatech.edu.
†Ph.D. Student, Guggenheim School of Aerospace Engineering, ypeng@gatech.edu
‡Associate Professor, Guggenheim School of Aerospace Engineering, wenting.sun@ae.gatech.edu.
§Assistant Professor, Woodruff School of Mechanical Engineering, AIAA Member, ellen.mazumdar@gatech.edu.

II. Quadrature Fringe Imaging Interferometer Diagnostic

At moderate to low temperatures, the relation between index of refraction n and density ρ for a gas is described by,

$$n - 1 = K(\lambda)\rho, \tag{1}$$

where $K(\lambda)$ is the wavelength dependent specific refractivity. For a mixture of gases, the effect of each species is summed together. Below 6000 K, the specific refractivity is largely independent of temperature and pressure and is often referred to as the Gladstone-Dale constant. At extreme conditions, however, the presence of ionized and dissociated species cause the specific refractivity to change with temperature and pressure [5]. In our previous work, we identified the shock tube conditions where the theoretical Gladstone-Dale would deviate from linear assumptions [15]. These shock tube simulations showed that regions with low driven gas pressures and high Mach numbers exhibit the largest deviations from linear theory and are easiest to achieve using conventional shock tube facilities. Therefore, these regions are of particular interest for initial experimental investigations. To reach higher temperatures and driven gas pressures, alternative topologies like free-piston shocktubes are needed.

To measure index of refraction, the QFII system utilizes two distinct interference fringe patterns from two types of sources: a narrowband source and a broadband source. In this scheme, the narrowband laser generates infinite interference fringes which functions as an analog quadrature to automatically track movement direction. The electric field interference calculations and index of refraction equations for the narrowband source are described in detail in [15]. In general, for two sinusoidal fringe signals α and β offset by a phase shift $\phi_{\alpha\beta}$, the change in index of refraction can be calculated for a single pass Mach-Zehnder interferometer from,

$$\Delta n = \frac{\lambda}{\pi W} tan^{-1}\left(\frac{\beta(\Delta n) + \alpha(\Delta n) sin(\phi_{\alpha\beta})}{\alpha(\Delta n) cos(\phi_{\alpha\beta})}\right), \tag{2}$$

where W is the internal window-to-window width of the shock tube and λ is the wavelength of the laser source. For this equation, the inverse tangent function must be unwrapped in order to accurately estimate larger index of refraction changes.

Since the quadrature equations rely on fringe movement to calculate the change in index of refraction, a reference index of refraction is necessary. Through the Ciddor equations [20], the wavelength dependent index of standard dry air, n_{as}, (15°C, 101.325 kPa, 0% relative humidity) is,

$$10^8(n_{as} - 1) = \frac{k_1}{k_0 - \sigma^2} + \frac{k_3}{k_2 - \sigma^2}. \tag{3}$$

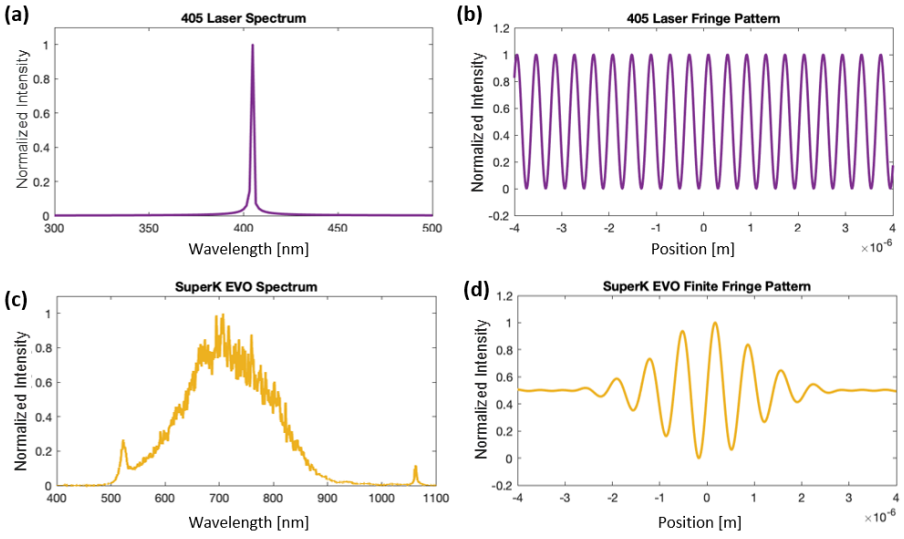

Fig. 1 (a) The narrowband 405 nm laser spectrum and (b) the nearly infinite interference fringes are shown. (c) In contrast, the SuperK EVO spectrum and (d) finite interference fringes with a strong center fringe are also illustrated.

Here, σ is the vacuum wave number $(1/\lambda_0)$, $k_0 = 238.0185\ um^{-2}$, $k_1 = 5792105\ um^{-2}$, $k_2 = 57.362\ um^{-2}$, and $k_3 = 167917\ um^{-2}$. Similarly, the index of pure standard water vapor (20 °C, 1.333 kPa) is,

$$10^8(n_{ws} - 1) = 1.022(w_0 + w_1\sigma^2 + w_2\sigma^4 + w_3\sigma^6), \tag{4}$$

where $w_0 = 295.235\ um^{-2}$, $w_1 = 2.6433\ um^{-2}$, $w_2 = -0.032380\ um^{-2}$, and $w_3 = 0.004028\ um^{-2}$. The combined temperature and pressure dependent group index of moist air is then,

$$n - 1 = \frac{\rho_a}{\rho_{as}}(n_{as} - 1) + \frac{\rho_w}{\rho ws}(n_{ws} - 1), \tag{5}$$

where ρ_a and ρ_w are the densities of the dry air component and water vapor respectively (found from the BIPM equation [21]), ρ_{as} is the density of standard dry air, and ρ_{ws} is the density of pure standard water vapor. These calculations are valid for -40 to 100 °C, 80 to 120 kPa, and 0 to 100% relative humidity. At ambient conditions in the laboratory (294 K, 97.73 kPa, 0% humidity, 450 ppm CO_2, λ = 405 nm), the reference index of refraction is $n_{amb} = 1.00026702$.

In contrast to narrowband sources, broadband source interference patterns create multi-color, finite fringe patterns with a strong black or white center fringe. Since these finite fringes only appear at the center of the interferometer, the center fringe functions as an absolute reference value. Sources with wide spectra will generate fewer finite fringes and stronger center fringes. Common broadband sources include LEDs, halogen bulbs, and flash lamps. However, these sources do not provide sufficient light for sampling rates greater than 200 kHz (2μs exposure) using a Shimadzu HPV-X2 ultra-high-speed camera. For ultra-high-speed shock tube experiments at sampling rates up to 5 MHz, we used a SuperK EVO supercontinuum white laser capable of emitting wavelengths from 400-2400 nm in a single spatially coherent beam. Figure 1 shows spectra and interference patterns for both the narrowband 405 nm laser source and the broadband SuperK EVO supercontinuum source.

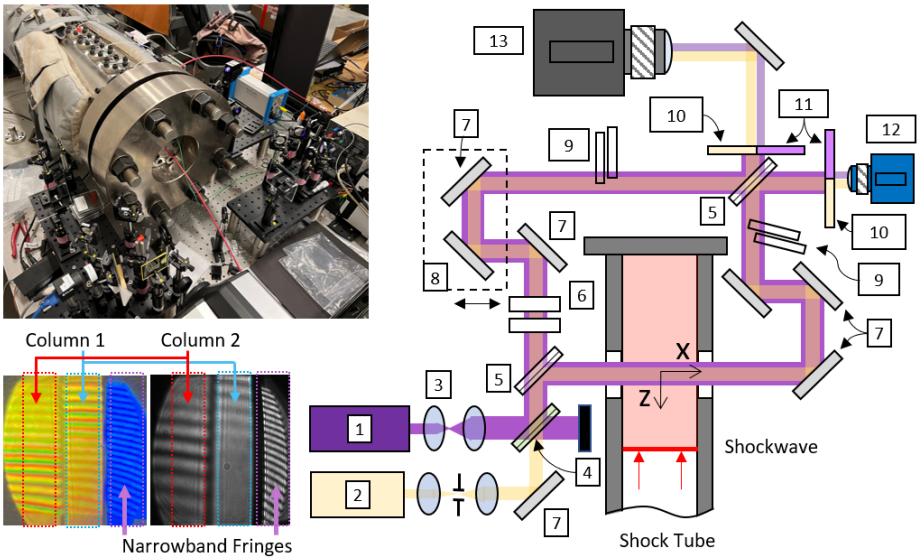

Fig. 2 The Mach-Zehnder configuration of the QFII diagnostic shows how narrowband and broadband sources can be combined to determine index of refraction changes inside a shock tube. A photo of the diagnostic setup is shown along with a color image and a black and white image of the fringe patterns. 1) 405 nm laser, 2) broadband source, 3) lenses, 4) 425 nm long pass dichroic, 5) 50/50 beam splitter, 6) windows to match delay, 7) broadband mirrors, 8) adjustable leg, 9) glass delay plates, 10) 420 nm long pass filter, 11) 425 nm short pass dichroic, 12) calibration camera, 13) ultra-high-speed camera.

III. Experimental Setup

The QFII diagnostic shown in Fig. 2 consists of a Mach-Zehnder interferometer with a continuous $\lambda = 405$ nm laser source and a 20 MHz pulsed Super K EVO HP EU-4 supercontinuum broadband source (410 to 2400 nm). The QFII can also be implemented as a double-pass Michelson interferometer for higher resolution; however, the Mach-Zehnder topology has more degrees of freedom enabling more parameters to be adjusted independently.

In Fig. 2, the two sources are first expanded with lenses and then combined with a longpass dichroic mirror. After passing through the 50/50 plate beam splitter, one leg travels through the shock tube. The free-space leg passes through two windows of identical thickness to the shock tube windows to match beam delay. For broadband light, inserting identical windows produces better fringe profiles than physically shortening the leg; this effect occurs due to differences in beam divergence through free space versus through the windows. The free-space leg also consists of mirrors on a micrometer stage, which is used to balance the lengths of the two interferometer legs. Additional glass plates can be inserted at tilted angles to split the broadband fringes into columns with different delays. With no tilted plates, the pressure range is dependent on the mirror tilt alone. With tilted plates, the range of pressures over which the center fringe is visible can be greatly increased. Depending on the expected fringe movement, the fringe spacing can be decreased by tilting the mirrors and delay plates. The interferometer center can also be set outside of the field of view to ensure that the center is visible after the shock-wave passes. Finally, the two legs are recombined with another matching 50/50 plate beam splitter and the sources are separated using a 420 nm long-pass colored glass filter and a shortpass 425 nm dichroic mirror. The fringe patterns are then imaged using an ultra-high-speed Shimadzu HPV-X2 camera (250 $\times$ 400 pixels, 10-bit monochrome, 128 or 256 frames) capable of capturing video up to 5 MHz (million frames per second) at full frame.

This QFII diagnostic is implemented on the Georgia Tech shock tube [22], which is a single diaphragm tube with an adjustable 6 or 10 m long driver section and 10 m long driven section. The tube is constructed out of 316 stainless steel and has a 15.24 cm inner diameter with a 5.08 cm wall thickness. The QFII diagnostic is passed through two circumferential ports located 1.24 cm away from the endwall. The sapphire windows of the ports are 12.7 mm in diameter and 3 mm thick with an optically clear opening that is approximately 10 mm in diameter. Four pressure transducers spaced un-equally along ports preceding the optical windows identify wave speed. The camera acquisition is triggered off a fifth pressure transducer immediately above the optical window.

IV. Calibration

To calibrate the diagnostic *in situ*, vacuum is first applied in the driven section of the shock tube. Because the Shimadzu HPV-X2 can only save batches of data once every few seconds, it is not well-suited for continuous calibrations. Therefore, a Blackfly monochrome camera (Blackfly S, BFS-U3-32S4M-C, 2048 $\times$ 1536 pixels, 12-bit, max 118 fps) is placed at the second output of the interferometer for calibration purposes. While pressure decreases in the driven section, the Blackfly camera runs continuously while the Shimadzu camera runs periodically every ~10 seconds to capture data. After collection, the data is recombined in order to calibrate the Shimadzu against the Blackfly. To monitor pressure, readings from a pressure gauge (Omega DPG4000, 0-300 psi, ± 0.25% vacuum accuracy) are collected with another

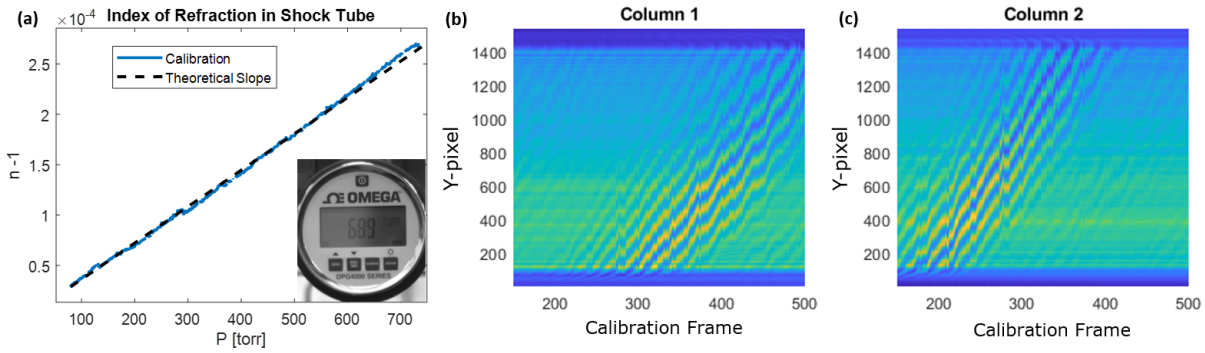

Fig. 3 (a) The experimental Gladstone-Dale calibration matches well with the quadrature signal. (b) The center fringe travels along each column at different frames, therefore covering a wider range of index values.

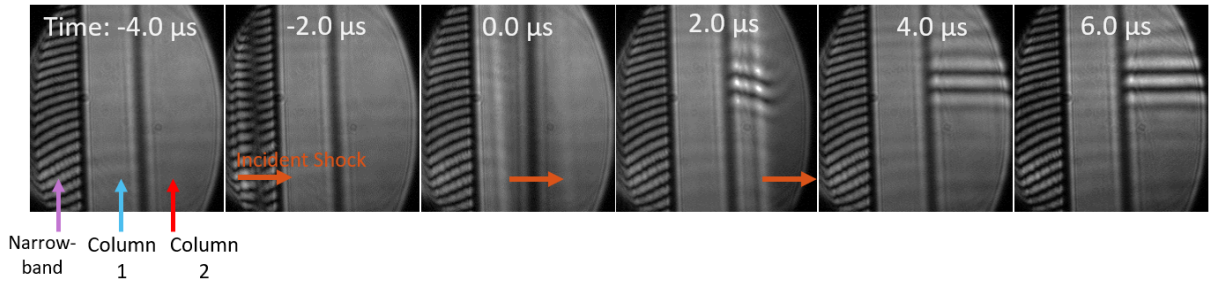

Fig. 4 The incident shock passes from left to right over a series of frames on the ultra-high-speed camera during a Mach 2.92 experiment. Center fringes are clearly visible in Column 2 after the shock passes.

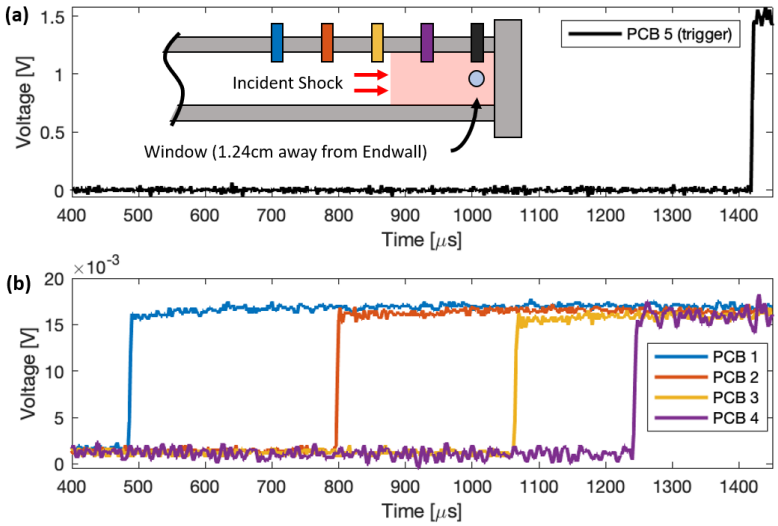

Fig. 5 (a) The high-speed camera is triggered off the pressure transducer above the window. (b) Signals from the tranducers preceding the window indicate wave speed.

Blackfly camera. Calibrations taken with the narrowband laser source show excellent agreement with the theoretical Gladstone-Dale value, as illustrated in Fig. 3(a). The basis of the inversion algorithm required to calculate index of refraction from discrete images is described in detail in [15]. However, the Blackfly and Shimadzu HPV-X2 cameras have different quantum efficiencies as a function of wavelength across the visible spectrum, so accurately comparing and automatically calculating fringe pattern across the cameras requires additional future consideration.

V. Results

Results from one shock tube experiment are shown in Fig. 4. In this experiment, the driven section was filled with air to 10.66 kPa and the driver was pressurized with helium. The scored aluminum diaphragm burst at 685 kPa, which generated an initial shock wave traveling at Mach 2.92. In Fig. 4(a), the shock wave can be clearly seen passing from left to right. Initially, no distinct center fringes are seen in either of the broadband columns. Once the wave front passes, dark fringes appear in the right column, indicating that a sudden change in index of refraction has occurred. This fringe pattern remains stable for the remainder of the video acquisition on the ultra-high-speed camera, indicating that the post-shock condition is constant. Fig.5 shows the pressure transducer signals used to trigger the camera and calculate wave speed. From normal shock relations, the theoretical temperature and pressure behind the initial shock are 794 K and 106.4 kPa, respectively.

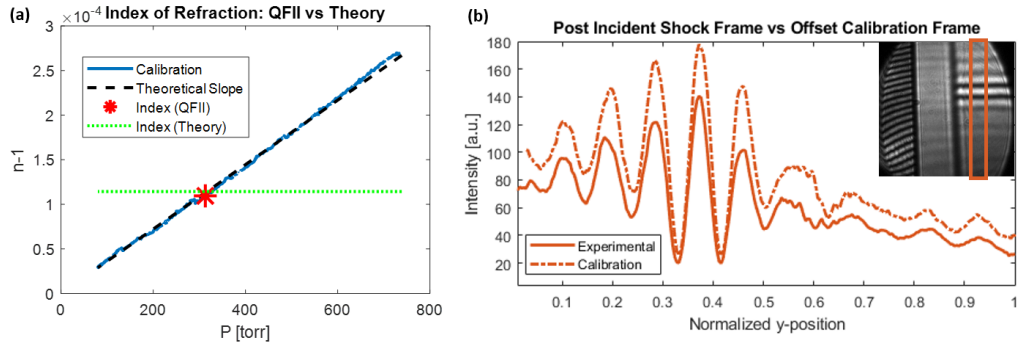

Fig. 6 (a) Index of refraction values from the QFII measurement and normal shock relations are shown, illustrating close agreement. (b) The broadband fringe profiles from the frame acquired after the incident shock wave and the frame acquired during calibration are also shown in close agreement.

To calculate the index of refraction, the post-incident shock frame is compared to the calibration maps. By comparing the broadband fringe profiles of each column, we find an estimated index of refraction from the nearest high-speed calibration frame. The fringe pattern can then be interpolated using the Blackfly frames or even between frames to increase accuracy. Compared to the theoretical index of refraction calculated from normal shock relations and the Ciddor equations, the QFII underestimates the index of refraction. The slight difference of 4.804×10^{-6} may be attributed to complex boundary layer effects within the tube. Additional uncertainties may arise from differences between the calibration camera and high-speed camera. Since the cameras are placed on either side of the final beam splitter, the fringe profile for one camera is the inverse of the other. The profiles are also not directly comparable due to the dissimilar sensor quantum efficiencies over the range of wavelengths. The accuracy and uncertainty of the QFII diagnostic are still unknown at this time. In the future, we plan to collect more data points and refine calibration techniques and post-processing algorithms to fully characterize the system.

VI. Conclusions and Future Work

The rapid change in index of refraction across a shock front is difficult to track since fringes can move on the order of tens to hundreds at extreme hypersonic conditions. In this paper, we demonstrate the QFII system that is capable of resolving large jumps in index of refraction with a modified Mach-Zehnder interferometer and two sources. The narrowband source provides high resolution and automated tracking while the broadband source acts as an absolute reference. If calibration maps are generated during the evacuation of the driven side, sudden changes in index of refraction can be resolved. Initial results from a shock tube experiment demonstrate that the broadband reference can be used to determine index of refraction, which closely matches the theoretical calculations. Further experiments will be conducted in order to determine the resolution and uncertainty of this diagnostic technique.

In future work, we also plan to collaborate with Sandia National Laboratories and their high-enthalpy free-piston shock tube capable of reaching high temperatures above 6000 K at moderate pressures [23, 24]. Measurements taken at the Sandia free-piston shock tube will be the first high-resolution index of refraction validation data above 6000 K, and will help create a validation database for index of refraction in non-equilibrium, compressible flows.

Acknowledgments

The authors would like to thank Dr. Daniel Guildenbecher and Dr. Kyle Lynch at Sandia National Labs for their insight and assistance with equipment. We would also like to thank members of the Sensing Technologies Laboratory for their assistance with algorithm development and diagnostic setup. The authors would like to acknowledge the Sandia National Laboratories Academic Alliance Laboratory Directed Research and Development (LDRD) program for funding this research. Sandia National Laboratories is a multimission laboratory managed and operated by National Technology and Engineering Solutions of Sandia, LLC., a wholly owned subsidiary of Honeywell International, Inc., for the U.S. Department of Energy's National Nuclear Security Administration under contract DE-NA0003525. The views expressed in the article do not necessarily represent the views of the U.S. Department of Energy or the United States Government.

References

[1] Gupta, A., and Argrow, B., "Analytical Approach for Aero-Optical and Atmospheric Effects in Supersonic Flow Fields," *AIAA Scitech 2020 Forum*, 2020. https://doi.org/10.2514/6.2020-0684.

[2] Owens, J. C., "Optical Refractive Index of Air: Dependence on Pressure, Temperature and Composition," *Appl. Opt.*, Vol. 6, No. 1, 1967, pp. 51–59. https://doi.org/10.1364/AO.6.000051.

[3] Osipov, A. I., Panchenko, V. Y., and Filippov, A. A., "Refractive Index of a Vibrationally Excited Gas," *Soviet Journal of Quantum Electronics*, Vol. 14, No. 9, 1984, pp. 1259–1260. https://doi.org/10.1070/qe1984v014n09abeh006205.

[4] Meggers, W., and Peters, C., "Measurements on the Index of Refraction of Air for Wave-Lengths from 2218 A to 9000 A," *The Astrophysical Journal*, Vol. 50, 1919, pp. 56–71.

[5] Kharitonov, A. I., Khoroshko, K. S., and Shkadova, V. P., "Temperature Dependence of Air Refraction at High Temperatures," *Fluid Dynamics*, Vol. 9, No. 5, 1974, pp. 851–853. https://doi.org/10.1007/BF01017444.

[6] Alpher, R. A., and White, D. R., "Optical Refractivity of High-Temperature Gases. II. Effects Resulting from Ionization of Monatomic Gases," *The Physics of Fluids*, Vol. 2, No. 2, 1959, pp. 162–169. https://doi.org/10.1063/1.1705907.

[7] Byron, S., "Shock-Tube Measurement of the Rate of Dissociation of Nitrogen," *The Journal of Chemical Physics*, Vol. 44, No. 4, 1966, pp. 1378–1388. https://doi.org/10.1063/1.1726870.

[8] Besse, A. L., and Kelley, J. G., "Interferometer for Shock Tube," *Review of Scientific Instruments*, Vol. 37, No. 11, 1966, pp. 1497–1499. https://doi.org/10.1063/1.1720027.

[9] Rowley, P. D., "A Laser Interferometer for Highly Transient Plasma Diagnostics," *Review of Scientific Instruments*, Vol. 41, No. 3, 1970, pp. 313–318. https://doi.org/10.1063/1.1684506.

[10] Spurk, J. H., and Bartos, J. M., "Interferometric Measurement of the Nonequilibrium Flow Field around a Cone," *The Physics of Fluids*, Vol. 9, No. 7, 1966, pp. 1278–1285. https://doi.org/10.1063/1.1761841.

[11] Cary, B., "Shock-Tube Study of the Thermal Dissociation of Nitrogen," *The Physics of Fluids*, Vol. 8, No. 1, 1965, pp. 26–35.

[12] Kashitani, M., Yamaguchi, Y., Miyazaki, D., and Oki, G., "A Modified Point-Diffraction Interferometry for Shock Tube Airfoil Testing," *50th AIAA Aerospace Sciences Meeting including the New Horizons Forum and Aerospace Exposition*, 2012. https://doi.org/10.2514/6.2012-468.

[13] Tanno, H., Itoh, K., Kento, Y., Yamada, K., Kobayashi, M., Shimamura, K., and Uchibe, G., "Flow Visualization with Common Path Interferometry in High-Enthalpy Shock Tunnel," *AIAA Scitech 2020 Forum*, 2020. https://doi.org/10.2514/6.2020-1281.

[14] Kiefer, J. H., and Manson, A. C., "Refractive Index Change and Curvature in Shock Waves by Angled Beam Refraction," *Review of Scientific Instruments*, Vol. 52, No. 9, 1981, pp. 1392–1396. https://doi.org/10.1063/1.1136779.

[15] Wang, G., and Mazumdar, Y. C., "High-Gradient Index of Refraction Measurements with a Quadrature Fringe Imaging Interferometer," *AIAA Scitech 2021 Forum*, 2021. https://doi.org/10.2514/6.2021-0936.

[16] Goossens, H. W. J., and Van Dongen, M. E. H., "Quantitative Laser-interferometric Measurement of Gas Density in a Gas-particle Mixture," Vol. 5, 1987, pp. 189–192. https://doi.org/10.1007/BF00298461.

[17] Buchenauer, C. J., and Jacobson, A. R., "Quadrature Interferometer for Plasma Density Measurements," *Review of Scientific Instruments*, Vol. 48, No. 7, 1977, pp. 769–774. https://doi.org/10.1063/1.1135146.

[18] Jacobson, A. R., and Call, D. L., "Novel Interferometer for the Measurement of Plasma Density," *Review of Scientific Instruments*, Vol. 49, No. 3, 1978, pp. 318–320. https://doi.org/10.1063/1.1135399.

[19] Wang, G., and Mazumdar, Y. C., "Quadrature Fringe Imaging Interferometer for Index of Refraction Measurements," *OSA Imaging and Applied Optics Conference: Laser Applications to Chemical, Security and Environmental Analysis*, 2020, p. LTh4F.2.

[20] Ciddor, P. E., "Refractive Index of Air: New Equations for the Visible and Near Infrared," *Appl. Opt.*, Vol. 35, No. 9, 1996, pp. 1566–1573. https://doi.org/10.1364/AO.35.001566, URL http://www.osapublishing.org/ao/abstract.cfm?URI=ao-35-9-1566.

[21] Davis, R. S., "Equation for the Determination of the Density of Moist Air (1981/91)," *Metrologia*, Vol. 29, No. 1, 1992, pp. 67–70. https://doi.org/10.1088/0026-1394/29/1/008, URL https://doi.org/10.1088/0026-1394/29/1/008.

[22] Karimi, M., Ochs, B., Liu, Z., Ranjan, D., and Sun, W., "Measurement of Methane Autoignition Delays in Carbon Dioxide and Argon Diluents at High Pressure Conditions," *Combustion and Flame*, Vol. 204, 2019, pp. 304–319. https://doi.org/10.1016/j.combustflame.2019.03.020.

[23] Lynch, K. P., and Wagner, J. L., "A Free-piston Driven Shock Tube for Generating Extreme Aerodynamic Environments," *AIAA Scitech 2019 Forum*, 2019. https://doi.org/10.2514/6.2019-1942.

[24] Petter, S. J., Lynch, K. P., Farias, P., Spitzer, S., Grasser, T., and Wagner, J. L., "Early Experiments on Shock-Particle Interactions in the High-Temperature Shock Tube," *AIAA Scitech 2020 Forum*, 2020. https://doi.org/10.2514/6.2020-0622.